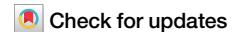
A Nature Portfolio journal



https://doi.org/10.1038/s43247-025-02509-5

# Rapid mineralisation of carbon dioxide in peridotites



Juerg M. Matter ® <sup>1</sup> ⊠, Joanna Speer ® <sup>1</sup>, Christopher Day ® <sup>2</sup>, Peter B. Kelemen ® <sup>3</sup>, Amal Ibrahim <sup>4</sup>, Sulaiman Al Mani <sup>4</sup>, Ehab Tasfai ® <sup>4</sup>, Moeez Ilyas <sup>4</sup>, Karan Khimji <sup>4</sup> & Talal Hasan <sup>4</sup>

The success of industrial scale carbon capture and storage in geologic reservoirs depends on the permanence of the stored carbon dioxide ( $CO_2$ ). Carbon dioxide capture and mineralisation (CCM) or mineral carbonation, which is the conversion of  $CO_2$  to carbonate minerals via fluid-rock reactions provides low risk and permanent  $CO_2$  removal. Here, we demonstrate rapid mineralisation of industrial  $CO_2$  emissions in mantle peridotites. Captured  $CO_2$  from an ammonia plant in the Sultanate of Oman has been injected into peridotite at a pilot test site in the Samail ophiolite. Chemical and isotopic results indicate rapid carbonate mineral precipitation. Mass balance calculations suggest that ~88% of the injected  $CO_2$  was mineralised as carbonate minerals within 45 days after injection. This successful approach of CCM unlocks peridotite as a promising new type of reservoir for the safe and permanent disposal of anthropogenic  $CO_2$  emissions.

Cumulative carbon dioxide emissions into the atmosphere have been estimated at  $2035 \pm 205$  GtCO<sub>2</sub> from 1870 to  $2019^{1}$ . To limit the impact of global warming and subsequent climate change, the Paris agreement recommended to limit average warming of the atmosphere to <2 °C, preferably to 1.5° compared to pre-industrial levels<sup>1</sup>. To reach this goal, the level of global carbon dioxide removal coupled with permanent storage must be approximately 10 Gt CO<sub>2</sub>/yr by 2050 and 20 Gt CO<sub>2</sub>/yr by 2100<sup>2</sup>. There are multiple storage options, with underground CO<sub>2</sub> storage in sedimentary formations being the most mature technique, with over 200 Mt of anthropogenic CO<sub>2</sub> being injected and stored in underground reservoirs for enhanced oil recovery by today<sup>3</sup>. Current estimates of aggregated global storage resources in underground reservoirs (mainly deep saline aquifers and depleted oil & gas reservoirs) are 13,954 GtCO<sub>2</sub><sup>4</sup>. In this type of reservoirs, CO<sub>2</sub> is primarily stored as supercritical or liquid CO<sub>2</sub>, with the tendency to migrate back to the surface due to buoyancy effects if not stored adequately. Another storage option is enhanced CO2 mineralisation in unconventional storage reservoirs, such as basalt and peridotite that mimics the natural process of silicate rock weathering<sup>5-12</sup>. In this approach, injected CO<sub>2</sub> reacts with mafic and ultramafic rocks, which contain high concentrations of calcium, magnesium, and iron, required for CO2 mineralisation. Combining CO<sub>2</sub> dissolution into water before or during the injection with insitu CO<sub>2</sub> mineralisation significantly increases storage permanence and security by immediate solubility trapping and subsequent mineralisation 13-15.

In-situ mineralisation in basalt has been successfully tested in a first pilot project in Iceland in 2012 $^{16}$ . A total of 230 tonnes of pure  $\rm CO_2$  and a  $\rm CO_2\textsc{-H}_2S$  mixture were injected fully dissolved in water into a basalt reservoir at 500 m depth $^{16}$ . Co-injection of non-reactive and reactive tracers, combined with detailed geochemical analysis of produced reservoir waters before, during and after the injection revealed rapid mineralisation of >95% of the injected  $\rm CO_2$  within less than two years  $^{17-19}$ . This storage technique has been further developed and implemented to a commercial scale by CarbFix, with >84 thousand tonnes of  $\rm CO_2$  injected since 2014 $^{20}$ . Theoretical global mineralisation potential in onshore and offshore basalt are on the order of several 100,000 GtCO<sub>2</sub> with a capacity of ~170 kg CO<sub>2</sub> per ton of basalt  $^{5,7,21-23}$ .

Ultramafic rocks, such as peridotites, provide the other main storage reservoir for in-situ mineralisation. Peridotites have a higher molar Mg to Si ratio and faster reaction kinetics with  $\rm CO_2$ -saturated fluids than basalt, making them an ideal candidate for mineralisation <sup>24–29</sup>. Peridotite is a major component of the Earth's upper mantle and is exposed in several large ophiolite massifs, such the Samail ophiolite in Oman and the United Arab Emirates. It is mainly composed of the minerals olivine, serpentine and brucite, which rapidly react with water containing  $\rm CO_2$ . Extensive natural  $\rm CO_2$  mineralisation has been observed in the Samail ophiolite with rates on the order of  $\rm 1000~tCO_2/km^3/yr^{6.25}$ . Recent studies showed that natural carbon mineralisation through weathering and groundwater circulation is limited to the upper tens of metres in the peridotite, with the deeper subsurface being  $\rm CO_2$  depleted<sup>29</sup>. Due to the disequilibrium of peridotite with

<sup>1</sup>School of Ocean and Earth Science, University of Southampton, Waterfront Campus, Southampton, UK. <sup>2</sup>Department of Earth Sciences, University of Oxford, Oxford, UK. <sup>3</sup>Lamont-Doherty Earth Observatory, Columbia University, New York, NY, USA. <sup>4</sup>Carbon Management Services SPC, Muscat, Sultanate of Oman. 

© e-mail: J.Matter@southampton.ac.uk

atmospheric  $CO_2$  and  $CO_2$ -saturated water below ~100 m depth, peridotites provide a large mineralisation reservoir with a theoretical mineralisation potential of  $10^5$ – $10^8$  GtCO<sub>2</sub> in Oman alone, and a capacity of 500–600 kg  $CO_2$  per ton of peridotite<sup>6,25</sup>.

To date, engineered  $CO_2$  mineralisation in peridotite has not been tested on a pilot scale. In this study, we use chemical and isotopic data from Project Chalk, the world's first in-situ  $CO_2$  mineralisation pilot in peridotites in the Samail ophiolite, Oman, to constrain the reaction kinetics of in-situ  $CO_2$ -water-rock reactions resulting in permanent  $CO_2$  mineralisation.

# Results Test site

The Oman Drilling Project (OmanDP) drilled multiple boreholes at the Oman Drilling Project Multi-borehole Observatory (MBO) in Wadi Lawayni, in the Tayin massif of the Oman ophiolite, approximately 25 km NE of Ibra, Oman (Fig. 1). The boreholes were drilled and fully characterized using wireline geophysical logging and hydrogeological testing by the Oman Drilling Project<sup>30,31</sup>. Core and drill cutting analysis indicate serpentinized dunite in the upper 100-250 m, and partially serpentinized harzburgite in the deeper part, with both rock types showing high density of mineralised veins<sup>29</sup>. Visual core description of continuous cores from boreholes BA1B and BA4A reveal that waxy green to white serpentines are the dominant vein minerals, whereas Ca-Mg carbonate filled veins are only found in the shallow part of the subsurface (<100 m)<sup>29</sup>. Borehole pumping tests using a straddle packer system revealed distinct zones of higher permeability with hydraulic conductivity values between  $1.6 \times 10^{-2}$  m/s (41–65 m below ground level interval, mbgl),  $2.5 \times 10^{-6}$  m/s (108–135 mbgl), and  $<2.3 \times 10^{-8}$  m/s  $(135-400 \text{ mbgl})^{31}$ . Wireline logging and discrete fluid sampling indicated a stratification of the aquifer in well BA1A with oxidized, pH ~8 and electrical conductivity of ~580 µS/cm fluids in the upper 65-150 m, and highly reduced, pH >10, and electrical conductivity of ~1800 µS/cm fluids below 150 m depth<sup>30,32</sup>. No such stratification occurs in well BA1D, which is ~16 m apart from BA1A, revealing the heterogeneity of the peridotite<sup>32</sup>. Groundwater in BA1D is highly reduced with a pH >10 and an electrical conductivity of 1720 µS/cm<sup>32</sup>.

For the Project Chalk B, we utilized one of the existing 400-metre-deep boreholes, BA1D, for a single-well ('huff-n-puff) push-pull tests (Fig. 1).

## 'Pull solution' chemical and isotopic results

We report the pre-injection chemical and isotopic composition of the groundwater (GW) and the injected solution (IS) in Table 1. GW represents

the ambient groundwater in the target injection interval, and the IS water is shallow groundwater, which was pumped prior to the injection and stored in a surface tank. We also report chemical and isotopic data from a postinjection time series of 'pull-solution' samples collected in well BA1D (Supplementary Table S2). The pre-injection groundwater in the isolate interval had a pH of 11.02, a Br tracer concentration below detection limit. (DIC = dissolved and the dissolved inorganic carbon  $CO_2 + HCO_3^- + CO_3^{2-}$ ) was 154.8 µmol/L, whereas the injected solution had a pH of 4.1, a Br- tracer concentration of 4.42 mmol/L, and a DIC concentration of 122.3 mol/L (Table 1). Stable carbon isotope ratio of the DIC ( $\delta^{13}C_{DIC}$ ) of GW and IS were -20.10 and -33.50% V-PDB, respectively (Table 1).

The pH in the reservoir at the beginning of the pull phase was 7.45 but steadily increasing to 9.50 with increasing pumping time (Supplementary Table S2). The chemical and isotopic composition of the extracted 'pullsolution' (Ca<sup>2+</sup>, Mg<sup>2+</sup>, Na<sup>+</sup>,  $\Sigma$ Si, DIC and  $\delta^{13}$ C<sub>DIC</sub>) evolved during the pull phase (Supplementary Table S2). Bromide decreased from 0.72 mmol/L at the beginning of the pumping to between 0.11 and 0.12 mmol/L due to mixing of the injected solution with the groundwater ('solution mixing') in the reservoir (Fig. 2). The total recovery of Br was 37.61% as estimated by dividing the mass of bromide recovered during the pull phase by the mass of bromide injected. Calcium concentration displayed a sharp increase from 0.55 to 2.01 mmol/L, whereas Mg<sup>2+</sup> concentration decreased from 2.64 to 0.08 mmol/L, almost reaching pre-injection groundwater concentration of 0.002 mmol/L (Fig. 3). Sodium concentration generally increased from 2.91 to 5.04 mmol/L (Fig. 3). Total dissolved silicon concentration ( $\Sigma$ Si) in the collected 'pull solution' samples, initially increased from 0.58 to 0.66 mmol/ L but subsequently decreased to 0.43 mmol/L, whereas measured DIC concentrations decreased from 6.37 to 0.084 mmol/l (Fig. 3). These trends indicate that other processes in addition to conservative 'solution mixing' between the injected fluid and the groundwater occurred following the injection of the CO<sub>2</sub>-saturated solution.

#### Host rock dissolution and mineral carbonation

The chemical and isotopic composition of the collected 'pull solution' samples from the injection reservoir indicate mixing and  $\mathrm{CO}_2$ -water-rock reaction processes. To differentiate between mixing and water-rock reaction processes occurring in the reservoir post-injection, we first determined the concentrations of dissolved ions of interest, assuming non-reactive solution-mixing. The mixing ratio of the groundwater and injected solution was determined using the measured concentration of bromide, the injected

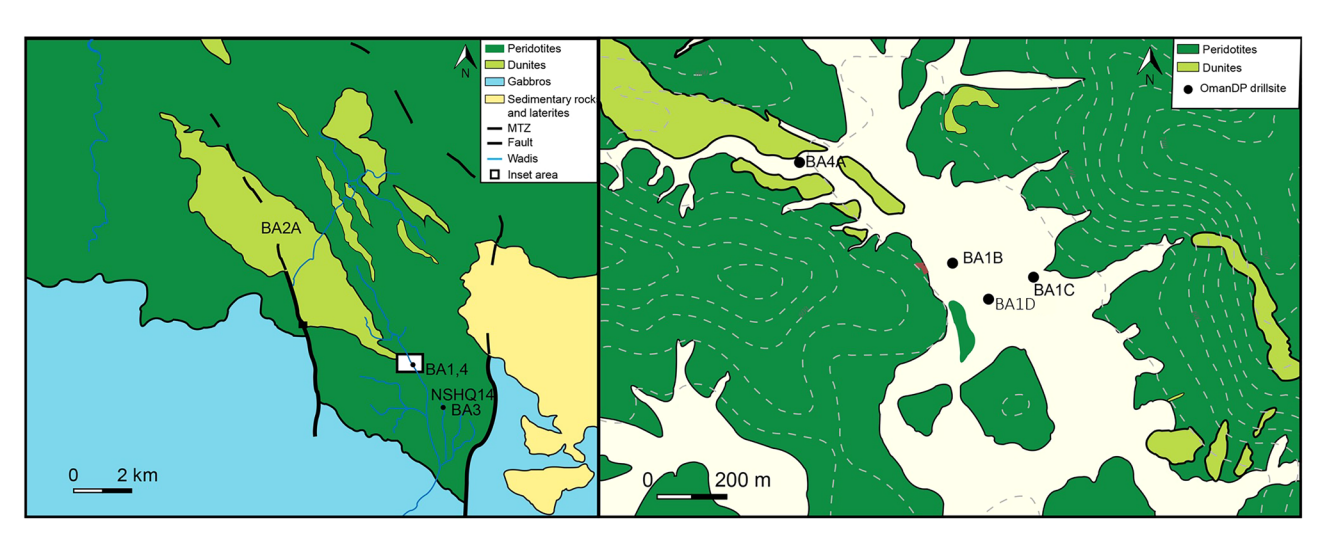


Fig. 1 | Geological maps of the Multi-borehole Observatory (MBO). The map on the left is a general geological map, showing the main rock formations, structural features (MTZ: Mantle Transition Zone) and borehole locations. The map on the

right is a specific map of the inset area, showing elevation contours as dashed grey lines (interval 5 m, from 550 to 590 masl) and the cluster of the BA boreholes.

non-reactive tracer (Supplementary Table S2). Subsequently, mass balance calculations were used (Eqs. (1) and (2)) to calculate the impact of non-reactive solution-mixing on the concentration of major dissolved ions (Supplementary Table S3, Fig. 3). Differences between the measured and the predicted concentrations (Eq. (3)) of these ions either suggest net dissolution (positive values) or net precipitation (negative values) (Supplementary Table S4).

Measured Mg and  $\Sigma$ Si concentrations were higher than the predicted ones during the pull phase, indicating an input of these elements via dissolution of the host rock. Measured Ca, Na and DIC concentrations were significantly lower than the ones predicted assuming non-reactive mixing, suggesting net-precipitation of secondary minerals (Fig. 3).

#### Mineral saturation states

Saturation indices (SI) of the collected fluid samples with respect to primary and secondary minerals are shown in Figs. 4 and 5. Primary silicate minerals present in the peridotite, such as forsterite and pyroxene (e.g. enstatite) were consistently undersaturated (Fig. 4). Various secondary silicate minerals from previous alteration (serpentine (chrysotile), brucite, chalcedony) show variable saturation states. Brucite was consistently undersaturated, whereas chrysotile was undersaturated at the beginning of the pull phase and oversaturated for the remaining pumping time. Chalcedony was close to saturation during the entire monitoring period. Key secondary minerals regarding CO<sub>2</sub> mineralisation, such as calcite and dolomite were at

Table 1 | Pre-injection conditions, cation, anion concentrations and stable carbon isotope ratio

Sample ID	Groundwater	Injection solution
•		35.00
T (°C)	35.20	35.00
pH	11.02	4.10
conductivity (mS/cm)	1.70	1.70
Ca (mmol/L)	3.61	1.73
Mg (mmol/L)	0.002	0.55
Na (mmol/L)	5.49	2.23
Si (mmol/L)	0.012	0.004
Br (mmol/L)	0.00	4.42
Br (ppm)	0.00	353.20
CI (mmol/L)	8.70	4.32
SO <sub>4</sub> <sup>2-</sup> (mmol/L)	0.57	0.60
DIC (mmol/L)	154.80	122,300.00
δ <sup>13</sup> C <sub>DIC</sub> (‰VPDB)	-20.10	-33.50

Fig. 2 | Bromide concentration in 'pull solution' samples post CO<sub>2</sub> injection. Bromide tracer concentrations measured in collected fluid samples from well BA1D after the dissolved CO<sub>2</sub> injection and 45 days of incubation period.

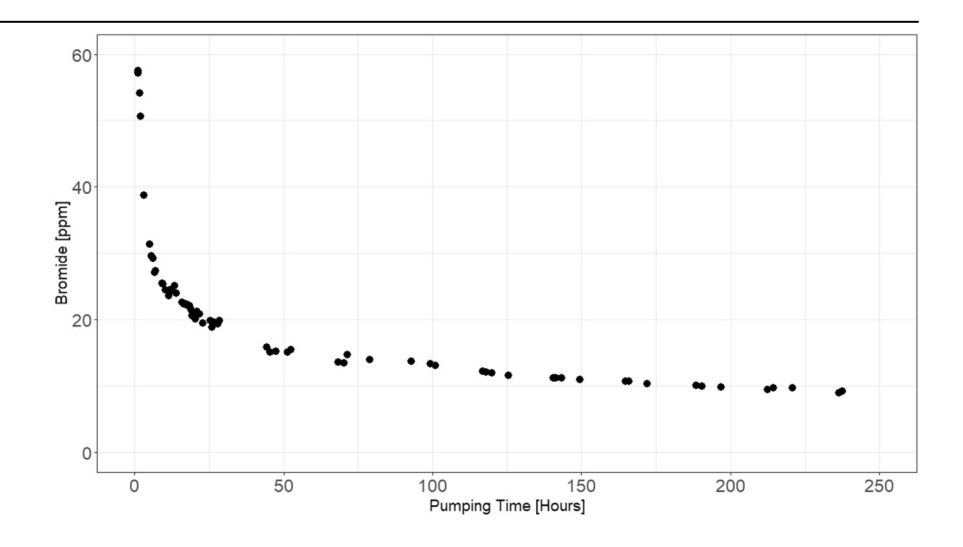
saturation or at supersaturation, whereas magnesite and hydromagnesite were undersaturated (Fig. 5).

#### **Discussion**

The evolution of the concentration of major elements, such as Ca, Mg, Na, Si as well as DIC reveal the effect of the  $CO_2$  reactivity. Differences between the measured and the calculated concentrations that assume non-reactive mixing, reveal mineral dissolution and precipitation reactions. Increasing Mg and  $\Sigma$ Si concentrations with positive computed  $\Delta$ Mg and  $\Delta$ Si values suggest a net input of these elements by dissolution of the host rock (Supplementary Table S4). Measured  $\Sigma$ Si concentrations initially increased and then slightly decreased but stayed higher than the predicted one for the whole duration of the pull phase, whereas the measured Mg concentration decreased during the pull phase but never reached the calculated concentration for non-reactive solution-mixing. Measured concentrations of Ca, Na and DIC decreased with increasing pumping time but were always below the calculated concentrations assuming non-reactive solution-mixing, as revealed by the negative  $\Delta$ Ca,  $\Delta$ DIC,  $\Delta$ Na, which indicate precipitation of secondary minerals (Supplementary Table S4).

# Fate of injected CO<sub>2</sub>

The chemical and isotopic composition of the extracted water samples reveal the reactivity of the injected CO2-saturated solution within the reservoir. Bromide was co-injected as a conservative, non-reactive tracer, and its volume integrated amounts recovered by pumping indicate a tracer recovery rate of 37.6%, meaning that we lost ~62% of Br (i.e. injected solution) through dispersion in the reservoir. Computed negative  $\Delta Ca$ ,  $\Delta$ DIC,  $\Delta$ Na values indicate precipitation, whereas positive  $\Delta$ Mg and  $\Delta$ Si values reveal dissolution reactions (Supplementary Table S4). The fate of the injected CO<sub>2</sub> is demonstrated by the DIC mass balance. The injected mass of DIC was 1011 moles and the amount of re-pumped DIC corrected for the dispersion within the reservoir using the Br recovery rate of 37.6% was 120 moles. Thus, 891 moles of DIC (88%) were lost by reaction processes during the 45 days of incubation time, confirming the non-conservative behaviour of DIC in the reservoir. Reaction processes, such as degassing of dissolved CO<sub>2</sub>, carbonate mineral dissolution or carbonate precipitation can change the total mass of inorganic carbon in the reservoir. Degassing of dissolved CO<sub>2</sub> from the injection reservoir can be excluded because the CO<sub>2</sub> was injected fully dissolved at a P<sub>CO2</sub> smaller than the hydrostatic head in the storage reservoir. Carbonate dissolution can also be excluded based on the negative  $\Delta$ DIC data. The most plausible process for the measured loss in DIC is carbonate mineral precipitation. This is supported by the saturation states of dolomite and calcite, two of the major carbonate phases that are commonly observed in weathered peridotites 25,26,33-35. Stable carbon isotope  $(\delta^{13}C_{DIC})$  in combination with DIC data provide further insight into the



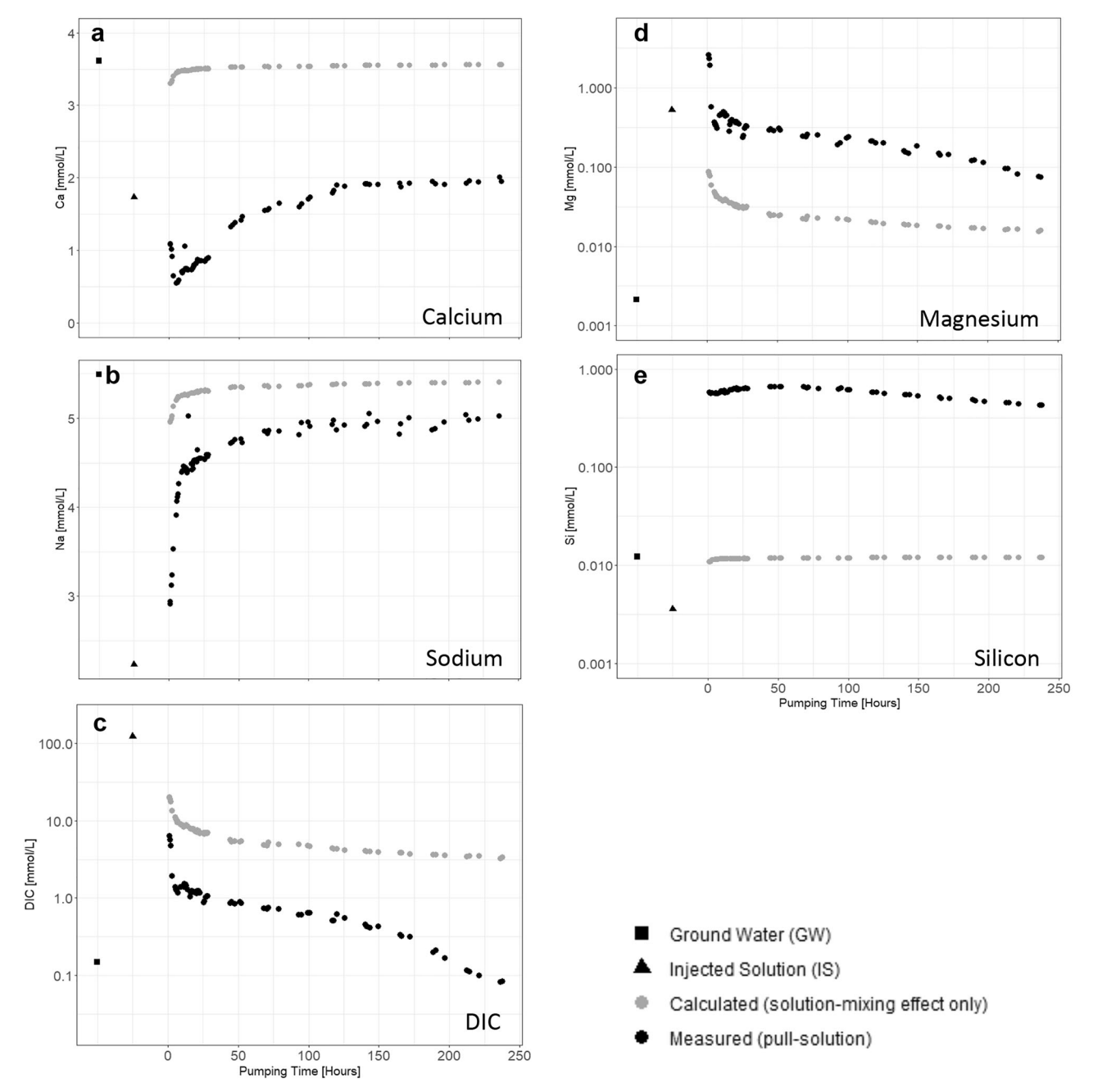


Fig. 3 | Time series of ion concentrations (predicted vs. measured) in 'pull solution' samples post CO<sub>2</sub> injection. a Measured and predicted calcium concentration vs. pumping time. b Measured and predicted sodium concentration vs. pumping time. c Measured and predicted DIC (dissolved inorganic carbon)

concentration vs. pumping time.  $\mathbf{d}$  Measured and predicted magnesium concentration vs. pumping time.  $\mathbf{e}$  Measured and predicted silicon concentration vs. pumping time.

governing geochemical processes and the  $CO_2$  reactivity  $^{36-39}$ . The baseline  $\delta^{13}C_{\rm DIC}$  prior to injection was -20.1% VPDB, and the injected  $CO_2$  saturated water had a  $\delta^{13}C_{\rm DIC}$  value of -33.50% VPDB, and thus is depleted by more than 10% in  $^{13}C$  compared to the baseline value (Fig. 6). Supplementary Table S2 shows that the  $\delta^{13}C_{\rm DIC}$  values of the collected water samples post-injection ranged from -32.47 to -36.97%. Comparing these measured values with the calculated ones based on non-reactive solution-mixing, yields negative  $\Delta\delta^{13}C_{\rm DIC}$  values (Supplementary Table S4). The trend to more negative  $\delta^{13}C_{\rm DIC}$  values in addition to the decreasing DIC concentration is indicative of carbonate mineral precipitation  $^{40}$ .

The data obtained during this pilot test and the saturation state calculations indicate precipitation of calcium carbonate or calciummagnesium carbonate minerals. The source of calcium is undetermined and could be carbonate minerals from pre-existing veins as well as Cabearing silicates in peridotite (e.g. pyroxenes and plagioclase) $^{2.5}$ . In addition, alkaline and carbon-depleted groundwater in the storage reservoir is enriched in Ca and mixing between the injected  $\rm CO_2$ -saturated solution and the alkaline groundwater results in direct  $\rm CO_2$  uptake via carbon mineralization $^{2.5}$ . Major contribution of calcium from Ca-carbonate-filled veins is unlikely due to a lack of carbonate minerals in veins in the target injection interval from 100 to 400 m depth. Thus, the likely source of Ca is from the dissolution of silicate minerals, as indicated by the increasing Si concentration post injection, and from the alkaline groundwater.

Overall, the results of this pilot study indicate rapid  $\mathrm{CO}_2$  mineralisation in peridotite. The acidic pH of the carbonated injection water was neutralized by solution-mixing with alkaline groundwater and by dissolution of

Fig. 4 | Saturation indices (SI) of major minerals. Calculated saturation indices (SI) of the collected fluid samples with respect to brucite, chalcedony, chrysotile, enstatite and forsterite. Positive, negative and zero SI values correspond to the fluids being supersaturated, undersaturated and at equilibrium with the specific mineral.

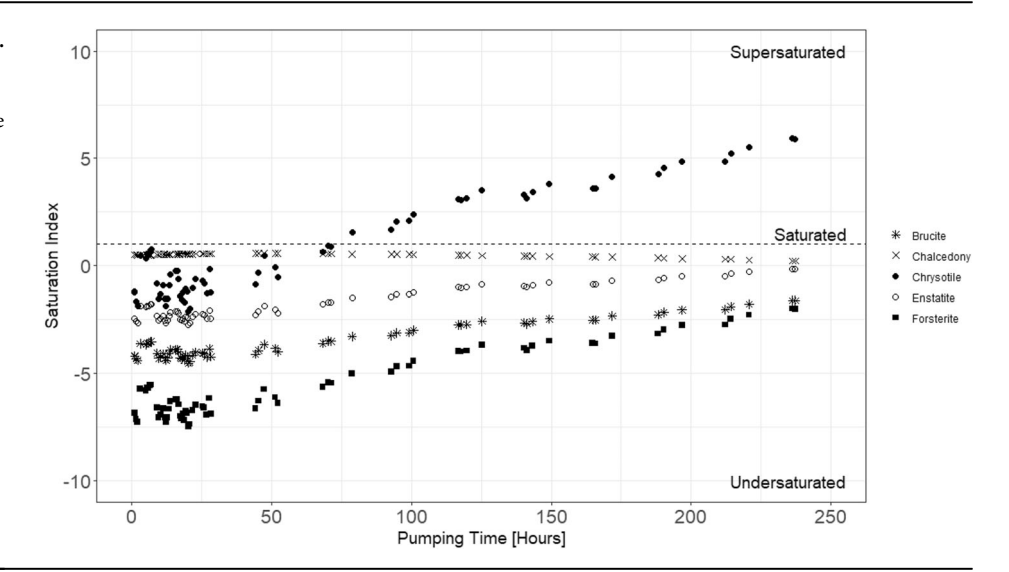
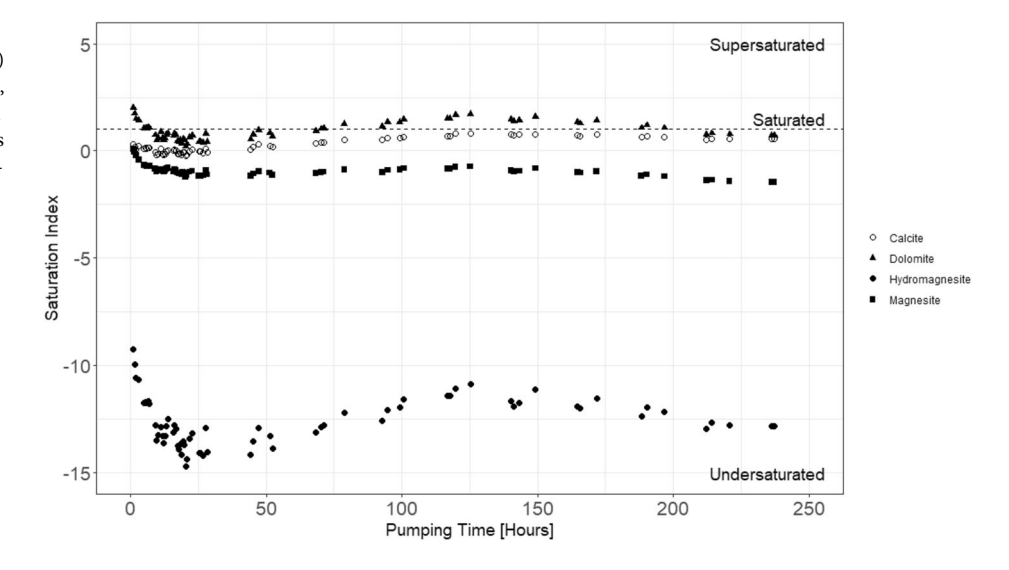


Fig. 5 | Saturation indices of major carbonbearing minerals. Calculated saturation indices (SI) of the collected fluid samples with respect to calcite, hydromagnesite, dolomite and magnesite. Positive, negative and zero SI values correspond to the fluids being supersaturated, undersaturated and at equilibrium with the specific mineral.



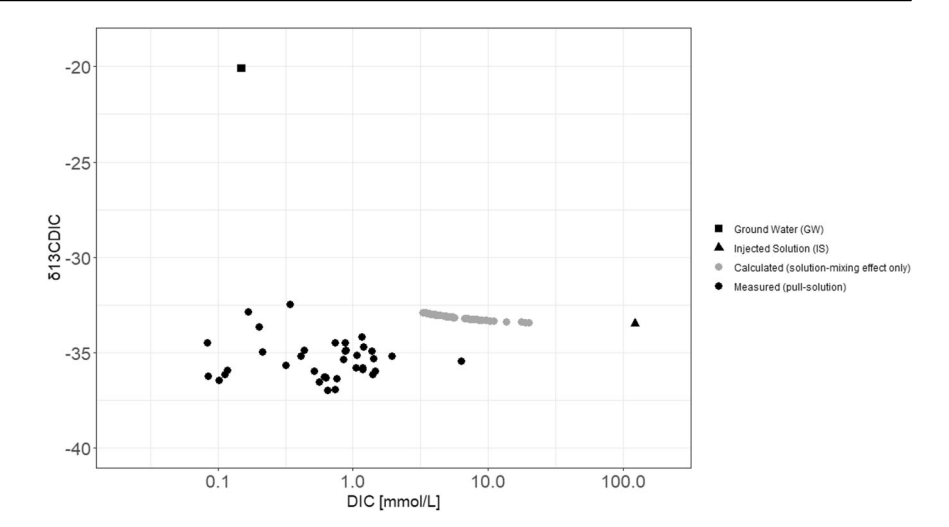
the host rock. This led to the precipitation of secondary carbonate minerals and to the storage of the injected CO<sub>2</sub>. CO<sub>2</sub> mineralisation rates in peridotite are faster than in basalt, which is likely due to its mineralogy, comprising of fast reacting minerals such as olivine, brucite, lizardite and chrysotile. The analysis of OmanDP core from the test site shows a high degree of serpentinization of the peridotite, with lizardite being the dominant serpentine polymorph and minor chrysotile in veins<sup>29</sup>. However, the alteration (hydration) and vein formation decrease with increasing depth, indicating fresher, potentially more reactive peridotite at greater depth<sup>29</sup>. Furthermore, CO<sub>2</sub> injection into peridotite aquifers, hosting alkaline, Ca-OH-rich groundwater, facilitates rapid carbonate precipitation. Using the collected chemical, stable carbon isotope, and tracer data in mass balance calculations provided quantitative information about in-situ reaction rates and the geochemical fate of the injected CO<sub>2</sub>.

This study, previous laboratory experiments and geologic evidence from natural analogues confirm rapid carbon mineralisation rates in peridotite<sup>6,24</sup>. However, porosity, permeability, injectivity and the coupled chemo-mechanical processes during mineralisation are almost unexplored<sup>27</sup>. Porosity measurements of discrete peridotite samples from OmanDP cores show decreasing porosity with increasing depth from maximum 16% in the shallow subsurface to 0.2% at depth<sup>41</sup>. Calculated permeability profiles based on resistivity data also decrease as a function of

depth from  $\sim 10^{-18}\,\mathrm{m}^2$  in the shallow subsurface (upper 150 m) to  $\sim 10^{-21}\,\mathrm{m}^2$  (>150–400 m). However, permeability and injectivity on a borehole to reservoir scale will be affected by the pervasive fracture network that is observed in peridotites. Injection into ultramafic rocks targets this pre-existing fracture network<sup>27</sup>. Scaling up CO<sub>2</sub> mineralisation in peridotite will depend on the accessibility of these fracture network, and most likely will require some kind of permeability enhancement and remobilization of the fracture network to get industrial scale injection rates.

Carbonation of peridotite results in an increase in solid volume, which could have negative or positive feedbacks. Decreasing permeability by clogging up available pore space is a potential negative feedback of carbonate precipitation in ultramafic rocks. However, natural alkaline springs in the peridotite, formed by hydration and carbonation reaction in the subsurface, persist for hundred thousands of years e.g. in Oman, without any indication of clogging up the reactive flow paths<sup>6,25,26</sup>. This could be explained by a positive feedback mechanism, such as "reaction-driven cracking". The solid volume increase due to carbonation can induce large differential stresses, which can cause fracturing and thus an increase in permeability and reactive surface area, both necessary to facilitate further rapid mineralisation<sup>42–45</sup>. What governs the different feedback mechanisms is unclear and currently an active field of research that requires coupled lab- and field experiments, as well as numerical approaches<sup>46</sup>.

Fig. 6 | Stable carbon isotope ratio ( $\delta^{13}C_{DIC}$ ) of dissolved inorganic carbon. Relationship between  $\delta^{13}C_{DIC}$  and DIC concentration in collected fluid samples after the incubation period of 45 days. Calculated values are the predicted concentrations and carbon isotopic composition based on non-reactive mixing (see Eq. (5)). The predicted values plot along a mixing hyperbola between the injected solution and the background reservoir fluid.



Given the limited volume of the injected  $\mathrm{CO}_2$  in this pilot test and all the uncertainties regarding injectivity, permeability and the coupled chemomechanical processes, further tests with significantly higher  $\mathrm{CO}_2$  injection volumes are necessary. Such tests are currently being conducted or are under development in the United Arab Emirates and the Sultanate of Oman.

#### Methods

## **Experimental procedure**

A single well push-pull test of a similar type described in Matter et al.8 and Assayag et al. 36 was conducted, whereby a CO<sub>2</sub>-saturated fluid was injected into a hydraulically isolated interval at 100-400 depth in well BA1D over a period of several hours using a borehole packer system. Prior to the CO<sub>2</sub> injection, groundwater was pumped out of well BA1D using a submersible pump and stored in a tank on the surface. In addition, groundwater samples were collected and chemically and isotopically analysed to establish a pre-CO<sub>2</sub> injection baseline. Subsequently, the groundwater in the tank was spiked with potassium bromide (KBr), which was used as a conservative (non-reactive) tracer, and sparged with CO<sub>2</sub> at ~9 atm in a closed system on the surface to form the injection solution (IS). Subsequently, the injection solution was injected ('push' phase) at a rate of 10 L/min and a pressure of 10-12 atm at surface into the hydraulic isolated interval in well BA1D below 100 m. The total mass of CO2 and water injected were 44.0 kg and 8220 litres, respectively. The test lasted for an incubation period of 45 days, during which the injected solution (IS) mixed with the groundwater (GW) via 'solution-mixing' in the reservoir and reacted ('chemical reaction') with the reservoir rocks. After the 45-day incubation period, the injected solution/groundwater mixture was pumped back ('pull' phase) from the hydraulically isolated interval in well BA1D using the packer system and a submersible pump and passed through a measurement cell in which pH, electrical conductivity, temperature, Eh and bromide concentrations were measured. The elapsed pumping time and the extracted fluid volume were recorded, and fluid samples collected from the 'pull-solution' for chemical and isotopic analysis.

#### Analytical methods

Mass balance calculations. Following the approach of Assayag et al.<sup>36</sup> and Matter et al.<sup>17</sup>, mixing fractions of the injected solution (IS) and the groundwater (GW) were calculated using following equation for bromide:

$$[Br]_i = X \cdot [Br]_{IS} + (1 - X) \cdot [Br]_{GW}$$
 (1)

The concentrations of the elements of interest (Ca, Mg, Na, Si) and DIC if no fluid-rock reactions and only non-reactive mixing occurred after the injection ( $C_i$ , predicted) were calculated using the bromide based mixing

fractions and following equation:

$$C_{i,predicted} = X_{Br} \cdot C_{i,IS} + (1 - X_{Br}) \cdot C_{i,GW}$$
 (2)

with  $C_i$  being the concentration of the ith component of interest (Ca, Mg, Na, Si or DIC) in the injection solution (IS), the groundwater (GW) and the predicted water after mixing.

Differences of concentrations of the elements of interest and DIC ( $C_i$ ) between the values measured in the collected fluid samples after the injection and the predicted values based on conservative mixing are defined as:

$$\Delta C_i = C_{i.measured} - C_{i.predicted} \tag{3}$$

Following mass balance equations were used to calculate the predicted  $\delta^{13}C_{\rm DIC}$  values  $^{36}\!\!:$ 

$$\begin{split} \delta^{13}C_{DIC,predicted} \cdot DIC_{predicted} = & X_{Br} \cdot DIC_{IS} \cdot \delta^{13}C_{DIC,IS} \\ & + (1 - X_{Br}) \cdot DIC_{GW} \cdot \delta^{13}C_{DIC,GW} \end{split} \tag{4}$$

which results in:

$$\delta^{13}C_{DIC,predicted} = \left[\frac{DIC_{IS} \cdot \delta^{13}C_{DIC,IS} - DIC_{GW} \cdot \delta^{13}C_{DIC,GW}}{DIC_{IS} - DIC_{GW}}\right] + \left[\frac{DIC_{BW} \cdot DIC_{IS} \left(\delta^{13}C_{DIC,GW} - \delta^{13}C_{DIC,IS}\right)}{DIC_{predicted} \cdot \left(DIC_{IS} - DIC_{GW}\right)}\right]$$
(5)

Mineral saturation states were calculated using PHREEQC programme<sup>47</sup>, the llnl database and the measured chemical composition, pH, temperature, and ionic strength of the collected fluid samples.

#### Fluid sample analyses

Concentrations of major ions were measured by inductively coupled plasma optical emission spectroscopy (ICP-OES) for cations using a Perkin-Elmer Optima 4300 DV and for anions by ion chromatography using a Dionex ICS2500, both at the National Oceanography Centre Southampton. Precision and accuracy of ICP-OES analyses based on repeated measurements of diluted in-house seawater standards is better than  $\pm 4\%$  for all the elements. For the anion analysis, repeated measurements of single anion standards indicate a precision better than  $\pm 1\%$  for Br and Cl analyses.

Dissolved inorganic carbon (DIC) analysis was completed using the VINDTA 3C (Marianda, Germany) at the National Oceanography Centre Southampton, using a coulometric titration (coulometer 5001, UIC, USA). All samples were analysed at 25 °C

(±0.1 °C) with temperature regulation using a water-bath (Julabo F12, Germany). Repeated measurements on the same batch of seawater ( $n \ge 3$ ) were undertaken every day prior to sample analysis, to assess the precision of the method, which was estimated for the whole dataset to be 1%. Certified Reference Materials (from A.G. Dickson, Scripps Institution of Oceanography) were analysed as standards to calibrate the instrument at the beginning and end of each day of analysis. A daily correction factor was applied to all measured values to standardize the results. Precision, calculated based on repeated measurements of the same in-house standard water samples, was 1%.

The carbon isotopic composition of the DIC samples ( $\delta^{13}C_{DIC}$ ) and gas samples  $(\delta^{13}C_{CO2(g)}, \delta^{18}O_{CO2(g)})$  were measured using a Delta V Advantage isotope ratio mass spectrometer (IRMS) fitted with a Gasbench II peripheral at the Department of Earth Science, University of Oxford, based on methods described by Assayag et al.<sup>48</sup>. The samples were calibrated with NBS-18 and NBS-19 calcite standards dissolved with 100% phosphoric-acid at 18 °C. For oxygen isotopes, an acid fractionation factor  $\alpha_{CO2(acid)-calcite} = 1.01053^{49}$ was used to correct for the difference in acid fractionation factor between the calcite standards and the gas samples. The relative 13C/12C values are reported in the conventional  $\delta^{13}$ C (‰) notation on the Vienna Pee Dee Belemnite (VPDB) scale, by assigning a value of +1.95% to NBS-19. The relative  $^{18}\text{O}/^{16}\text{O}$  values are reported in the conventional  $\delta$   $^{18}\text{O}$  (‰) notation on the VSMOW-SLAP scale such that the  $\delta^{18}$ O of SLAP water was -55.5%. Precision of δ<sup>13</sup>C<sub>DIC</sub>, based on repeat measurements of in-house standard NOCZ-DIC was  $\pm 0.16\%$  (1 $\sigma$ , n = 16), with average  $\delta^{13}C_{DIC} = 2.16\%$ within uncertainty of the long-term average of NOCZ-DIC (2.19‰). Precision of  $\delta^{13}C_{CO2(g)}$ ,  $\delta^{18}O_{CO2(g)}$  were 0.03% and 0.05% (1 $\sigma$ , n = 4) respectively.

# **Data availability**

All data required to evaluate the conclusions in the paper are available from Open Science Framework https://doi.org/10.17605/OSF.IO/5KGW.

Received: 8 September 2023; Accepted: 23 June 2025; Published online: 26 July 2025

# References

- IPCC. In Climate Change 2023: Synthesis Report. Contribution of Working Groups I, II and III to the Sixth Assessment Report of the Intergovernmental Panel on Climate Change (eds, Core Writing Team, Lee, H. & Romero, J.) (IPCC, 2023) pp. 35–115, https://doi.org/10. 59327/IPCC/AR6-9789291691647.
- National Academies of Sciences Engineering and Medicine. Negative emissions technologies and reliable sequestration: a research agenda (The National Academies Press, 2019). Available online at: https:// www.nap.edu/catalog/25259/negative-emissions-technologiesand-reliablesequestration-a-research-agenda.
- 3. Global CCS Institute. CO2RE database (Global CCS Institute, 2022).
- OGCI, Global CCS Institute, Storegga. CO<sub>2</sub> storage resources catalogue Cylce 3 Report (OGCI, Global CCS Institute, 2022). Available online at: https://www.ogci.com/wpcontent/uploads/2022/ 03/CSRC\_Cycle\_3\_Main\_Report\_Final.pdf.
- Goldberg, D. S., Takahashi, T. & Slagle, A. L. Carbon dioxide sequestration in deep-sea basalt. *Proc. Natl. Acad. Sci. USA* 105, 9920–9925 (2008).
- Kelemen, P. B. & Matter, J. In situ carbonation of peridotite for CO<sub>2</sub> storage. Proc. Natl. Acad. Sci. USA 105, 17295–17300 (2008).
- McGrail, B. P. et al. Potential for carbon dioxide sequestration in flood basalts. J. Geophys. Res. 111, B12201 (2006).
- Matter, J. M., Takahashi, T. & Goldberg, D. Experimental evaluation of in situ CO<sub>2</sub>-water-rock reactions during CO<sub>2</sub> injection in basaltic rocks: implications for geological CO<sub>2</sub> sequestration. Geochem. Geophys. Geosyst. 8, Q02001 (2007).
- Oelkers, E. H., Gislason, S. R. & Matter, J. Mineral carbonation of CO<sub>2</sub>. *Elements* 4, 333–337 (2008).

- Snæbjörnsdóttir, S. O. et al. Carbon dioxide storage through mineral carbonation. Nat. Rev. Earth Environ. 1. 90–102 (2020).
- Ferreira, A. et al. Unraveling the rapid CO<sub>2</sub> mineralization experiment using the Paraná flood basalts of South America. Sci. Rep. 14, 8116 (2024).
- Oelkers, E. H. et al. The subsurface carbonation potential of basaltic rocks from the Jizan region of Southwest Saudi Arabia. *Int. J. Greenh. Gas Control* 120, 103772 (2022).
- McMillan, B. & Bryant, S. L. Surface dissolution: minimizing groundwater impact and leakage risk simultaneously. *Energy Proc.* 1, 3707–3715 (2009).
- Gunnarson, I. et al. The rapid and cost-effective captures and subsurface mineral storage of carbon and sulfur at the CarbFix2 site. Int. J. Greenh. Gas Control 79, 117–126 (2018).
- Sigfusson, B. et al. Solving the carbon-dioxide buoyancy challenge: the design and field testing of a dissolved CO<sub>2</sub> injection system. *Int. J. Greenh. Gas Control* 37, 213–219 (2015).
- Gislason, S. R., Sigurdardóttir, H., Aradóttir, E. S. & Oelkers, E. H. A brief history of CarbFix: challenges and victories of the project's pilot phase. *Energy Procedia* 146, 103–114 (2018).
- Matter, J. M. et al. Rapid carbon mineralization for permanent disposal of anthropogenic carbon dioxide emissions. *Science* 352, 1312–1314 (2016).
- Pogge von Strandmann, P. A. E. et al. Rapid CO<sub>2</sub> mineralisation into calcite at the CarbFix storage site quantified using calcium isotopes. *Nat. Commun.* 10, 1983 (2019).
- Snæbjörnsdóttir, S. O. et al. The chemistry and saturation states of subsurface fluids during the in situ mineralisation of CO<sub>2</sub> and H<sub>2</sub>S at the CarbFix site in SW-Iceland. *Int. J. Greenh. Gas Control* 58, 87–102 (2017).
- Clark, D. E. et al. CarbFix2: CO<sub>2</sub> and H<sub>2</sub>S mineralization during 3.5 years of continuous injection into basaltic rocks at more than 250 °C. Geochim. Cosmochim. Acta 219, 45–66 (2020).
- Callow, B., Falcon-Suarez, I., Ahmed, S. & Matter, J. Assessing the carbon sequestration potential of basalt using X-ray micro-CT and rock mechanics. *Int. J. Greenh. Gas Control* 70, 146–156 (2018).
- Kelemen, P., Benson, S. M., Pilorgé, H., Psarras, P. & Wilcox, J. An overview of the status and challenges of CO<sub>2</sub> storage in minerals and geological formations. *Front. Clim.* 1, 9 (2019).
- Marieni, C., Henstock, T. J. & Teagle, D. A. H. Geological storage of CO<sub>2</sub> within the oceanic crust by gravitational trapping. *Geophys. Res.* Lett. 40, 6219–6224 (2013).
- Gadikota, G. et al. Elucidating the differences in the carbon mineralization behaviors of calcium and magnesium bearing aluminosilicates and magnesium silicates for CO<sub>2</sub> storage. Fuel 277, 117900 (2020).
- Kelemen, P. B. et al. Rate and mechanisms of mineral carbonation in peridotite: natural processes and recipes for enhanced, in situ CO<sub>2</sub> capture and storage. *Annu. Rev. Earth Planet. Sci.* 39, 545–576 (2011).
- Mervine, E. M. et al. Carbonation rates of peridotite in the Samail Ophiolite, Sultanate of Oman, constrained through 14C dating and stable isotopes. Geochim. Cosmochim Acta 126, 371–397 (2014).
- Mahzari, P. et al. Characterizing flow paths in peridotite formations for CO2 sequestration: hydro-mechanical modelling of a pilot test in the UAE. SPE-CCUS 4188767, https://doi.org/10.15530/ccus-2025-4188767 (2025).
- Nisbet, H. et al. Carbon mineralization in fractured mafic and ultramafic rocks: a review. Rev. Geophys. 62(4) https://doi.org/10. 1029/2023RG000815 (2024).
- Kelemen, P. B. et al. Initial results from the Oman Drilling Project Multi-Borehole Observatory: petrogenesis and ongoing alteration of mantle peridotite in the weathering horizon. *J. Geophys. Res. Solid Earth*, 125, https://doi.org/10.1029/2021JB022729 (2021).
- Kelemen, P. B., Matter, J. M., Teagle, D. A. H., Coggon, J. A. The Oman Drilling Project Science Team 2020. Proceedings of the Oman Drilling

- *Project: College Station, TX* (International Ocean Discovery Program, 2020). https://doi.org/10.14379/OmanDP.proc.2020.
- Lods, G. et al. Groundwater flow characterization of an ophiolitic hardrock aquifer from cross-borehole multi-level hydraulic experiments. *J. Hydrol.* 589, 125152 (2020).
- Nothaft, D. B. et al. Aqueous geochemical and microbial variation across discrete depth intervals in a peridotite aquifer assessed using a packer system in the Samail Ophiolite, Oman. J. Geophys. Res. Biogeosci. 126, https://doi.org/10.1029/2021JG006319 (2021).
- Chavagnac, V., Monnin, C., Ceuleneer, G., Boulart, C. & Hoareau, G. Characterization of hyperalkaline fluids produced by low-temperature serpentinization of mantle peridotites in the Oman and Ligurian ophiolites. *Geochem. Geophys. Geosyst.* 14, 2496–2522 (2013).
- Lacinska, A. M. et al. An experimental study of the carbonation of serpentinite and partially serpentinised peridotites. *Front. Earth Sci.* 5, https://doi.org/10.3389/fearth.2017.00037 (2017).
- Ternieten, L., Früh-Green, G. L. & Bernasconi, S. M. Carbon geochemistry of the active serpentinization site at the Wadi Tayin Massif: insights from the ICDP Oman Drilling Project: Phase II. J. Geophys. Res. Solid Earth, 126, https://doi.org/10.1029/ 2021JB022712 (2021).
- Assayag, N., Matter, J., Ader, M., Goldberg, D. & Agrinier, P. Water-rock interactions during a CO<sub>2</sub> injection field-test: implications on host rock dissolution and alteration effects. *Chem. Geol.* 265, 227–235 (2009).
- Emberley, S. et al. Monitoring of fluid-rock interaction and CO<sub>2</sub> storage through produced fluid sampling at the Weyburn CO<sub>2</sub>-injection enhanced oil recovery site. Saskatchewan, Canada. *Appl. Geochem.* 20, 1131–1157 (2004).
- Johnson, J. W., Nitao, J. J. & Knauss, K. G. reactive transport modelling of CO<sub>2</sub> storage in saline aquifers to elucidate fundamental processes, trapping mechanisms and sequestration partitioning. In: *Geological* storage of carbon dioxide (eds, Baines, S. J. & Worden, R. H.) 233, pp. 107–127 (Geological Society London Special Publications, 2004).
- Raistrick, M. et al. Using chemical and isotopic data to quantify ionic trapping of injected carbon dioxide in oil field brines. *Environ. Sci. Technol.* 40, 6744–6749 (2006).
- Clark, I. D. & Fritz, P. E. Environmental isotopes in hydrogeology, 1<sup>st</sup> edn. (CRC Press, 1997).
- Katayama, I. et al. And the Oman Drilling Project Phase 2 Science Party. Permeability profiles across the crust-mantle sections in teh Oman Drilling Project inferred from dry and wet resisitivity data. *J. Geophys. Res. Solid Earth* 125, e2019JB018698 (2020).
- Evans, O., Spiegelman, M. & Kelemen, P. B. Phase-field modeling of reaction-driven cracking: determining conditions for extensive olivine serpentinization. J. Geophys. Res. 125, e2019JB018614 (2020).
- 43. Jamtveit, B., Malthe-Sorenssen, A. & Kostenko, O. Reaction enhanced permeability during retrogressive metamorphism. *Earth Planet. Sci. Lett.* **267**, 620–627 (2008).
- Kelemen, P. B. & Hirth, G. Reaction-driven cracking during retrograde metamorphism: olivine hydration and carbonation. *Earth Planet. Sci. Lett.* 345-348, 81–89 (2012).
- 45. Zhu, W. et al. Experimental evidence of reaction-induced fracturing during olivine carbonation. *Geophys. Res. Lett.* **43**, 9535–9543 (2016).
- 46. Plümper, O. & Matter, J. Olivine the alteration rock star. *Elements* 19, 165–172 (2023).
- Parkhurst, D. L. & Appelo, C. A. J. Description of input and examples for PHREEQC Version 3 – a computer program for speciation, batchreaction, one-dimensional transport, and inverse geochemical calculations. In US Geological Survey Techniques and Methods Book, p. 497 (U.S. Geological Survey, 2013).
- Assayag, N., Rivé, K., Ader, M. & Agrinier, P. Improved method for isotopic and quantitative analysis of dissolved inorganic carbon in natural water samples. *Rapid Commun. Mass Spectrom* 20, 2243–2251 (2006).

 Kim, S.-T., Coplen, T. B. & Horita, J. Normalization of stable isotope data for carbonate minerals: implementation of IUPAC guidelines. *Geochim. Cosmochim. Acta* 158, 276–289 (2015).

# **Acknowledgements**

The project received funding from the ClimateWorks Foundation (Fluxx Grant # G-21030802317354, grant no. 21-1839). Boreholes and borehole straddle packer system used for the experiments were funded through the Oman Drilling Project, which was supported by the Alfred P. Sloan Foundation (in association with the Deep Carbon Observatory, DCO), the International Continental Scientific Drilling Program (ICDP), US National Science Foundation (NSF; grants # NSF-EAR-1516300, EAR-1516313), the Japanese Marine Science and Technology Center (JAMSTEC), the Japanese Society for the Promotion of Science (JSPS; grant # 16H06347) and the European Research Council.

## **Author contributions**

Conceptualization: J.M. Matter, A. Ibrahim, S. Al Mani, E. Tasfai. Funding acquisition: J.M. Matter, T. Hasan, K. Khimji. Investigation: J.M. Matter, J. Speer, C. Day, P. B. Kelemen, A. Ibrahim, S. Al Mani, E. Tasfai, M. Ilyas. Writing: J.M. Matter, J. Speer.

## **Competing interests**

The authors declare following competing interests: Co-authors Hasan, Tasfai and Khimji are inventors on patent US17/705,792 and EP22175231,4A, 'System and method for permanent carbon dioxide sequestration using a renewable energy source'. Columbia University, Kelemen and Matter hold US Patent 8524152, 'Systems and methods for enhancing rates of in situ carbonation in peridotite'. All other authors have no competing interests to declare.

#### Additional information

**Supplementary information** The online version contains supplementary material available at https://doi.org/10.1038/s43247-025-02509-5.

**Correspondence** and requests for materials should be addressed to Juerg M. Matter.

**Peer review information** Communications Earth & Environment thanks Alioja Lacinska, Jiajie Wang and the other, anonymous, reviewer(s) for their contribution to the peer review of this work. Primary Handling Editor: Joe Aslin. A peer review file is available.

**Reprints and permissions information** is available at http://www.nature.com/reprints

**Publisher's note** Springer Nature remains neutral with regard to jurisdictional claims in published maps and institutional affiliations.

Open Access This article is licensed under a Creative Commons Attribution 4.0 International License, which permits use, sharing, adaptation, distribution and reproduction in any medium or format, as long as you give appropriate credit to the original author(s) and the source, provide a link to the Creative Commons licence, and indicate if changes were made. The images or other third party material in this article are included in the article's Creative Commons licence, unless indicated otherwise in a credit line to the material. If material is not included in the article's Creative Commons licence and your intended use is not permitted by statutory regulation or exceeds the permitted use, you will need to obtain permission directly from the copyright holder. To view a copy of this licence, visit <a href="https://creativecommons.org/licenses/by/4.0/">https://creativecommons.org/licenses/by/4.0/</a>.

© The Author(s) 2025